Liu *et al. Cell & Bioscience* (2026) 16:31
https://doi.org/10.1186/s13578-026-01530-1

Cell & Bioscience

RESEARCH Open Access

The cytoskeleton regulates cytoophidium dynamics in *Drosophila* ovaries

Xiao-Jing Liu[1], Yi-Lan Li[1], Shu-Yu Pang[1], Ji-Long Liu[1,2*] and Kun Dou[1*]

Abstract
Cytoophidia are filamentous structures composed of CTP synthase (CTPS) and were first identified in the ovarian cells of *Drosophila*. As a highly conserved, membraneless organelle present across all three domains of life, cytoophidia exhibit dynamic behaviors essential for cellular homeostasis and function. Previous studies have demonstrated that cytoophidia are actively transported from nurse cells to the oocyte, suggesting a potential role in *Drosophila* oogenesis; however, the molecular and cellular mechanisms governing cytoophidium dynamics remain poorly understood. In this study, we employ live-cell imaging to systematically characterize the spatiotemporal dynamics of cytoophidia and to investigate the underlying regulatory mechanisms. Our findings reveal that cytoophidium dynamics depend on key cytoskeletal components, including microtubules, microfilaments, and myosin II. Disruption of either microtubules or microfilaments results in the disassembly or depolymerization of macro-cytoophidia, underscoring the essential role of the cytoskeleton in maintaining cytoophidium integrity and facilitating proper assembly. Collectively, these results establish that microtubules, microfilaments, and myosin II are pivotal for regulating cytoophidium dynamics. This study provides novel insights into the mechanisms of cytoophidium transport and assembly, and lays a foundation for further investigation of their functional significance in *Drosophila* oogenesis.

Keywords Cytoophidium, Cytoskeleton, Dynamics, Microtubule, Microfilament, Myosin II, *Drosophila* ovary, Oogenesis

Introduction

Cytidine-5′-triphosphate (CTP) is a key nucleotide that plays essential roles in phospholipid metabolism, and energy transfer. The *de novo* synthesis of CTP is catalyzed by CTP synthase (CTPS) [1]. In 2010, CTPS was discovered to form elongated, filamentous structures that are visible under light microscopy in *Drosophila* ovaries [2]. Shortly thereafter, similar filamentous CTPS assemblies were independently reported in the bacterium *Caulobacter crescentus* [3], and the yeast *Saccharomyces cerevisiae* [4]. Since these pioneering discoveries, cytoophidia have been identified in a wide range of organisms, including human cells [5, 6], fission yeast [7], plants [8], and archaea [9], underscoring their remarkable evolutionary conservation across the three domains of life [10–12].

Emerging evidences suggest the involvement of cytoophidia in a variety of cellular processes, such as protein homeostasis and lifespan regulation [13, 14], developmental switch [15, 16], cell adhesion [17], brain development [15], maintenance of cell polarity [18], intracellular transport [19], immune cell differentiation

*Correspondence:
Ji-Long Liu
liujl3@shanghaitech.edu.cn; jilong.liu@dpag.ox.ac.uk
Kun Dou
doukun@shanghaitech.edu.cn
[1]School of Life Science and Technology, ShanghaiTech University, Shanghai 201210, China
[2]Department of Physiology, Anatomy and Genetics, University of Oxford, Oxford OX1 9 3PT, UK

[20], oncogenesis [21], stress responses [9], and extracellular matrix regulation [22]. These findings point to the potential involvement of cytoophidia in diverse aspects of cellular physiology and adaptation [10–12, 23]. Cytoophidium assembly can be considered as one of the primary partitioning principles of the cell [24].

In *Drosophila* ovaries, cytoophidia are present in all three major cell types: nurse cells, oocytes, and follicle cells [25]. The polymerization of CTPS into cytoophidia has been shown to support egg production, an effect that becomes particularly evident when flies are exposed to the antimetabolite DON (6-diazo-5-oxo-l-norleucine), an inhibitor of CTP synthesis [5, 25, 26]. This observation highlights the important contribution of cytoophidia to oogenesis and suggests a functional link between CTP metabolism and cytoophidium integrity.

Furthermore, our previous work has demonstrated that cytoophidia in the *Drosophila* ovary are capable of active transport from nurse cells to oocytes through ring canals [27]. The intercellular trafficking for nurse cells to the oocyte is believed to facilitate the transfer of organelles, mRNAs, and proteins required for oocyte growth [28]. However, the molecular and cellular mechanisms that govern the directional transport and dynamic behavior of cytoophidia remain poorly defined.

In multicellular organisms, the precise transport and spatial organization of organelles are essential for normal cellular development and the execution of physiological functions [29]. Each *Drosophila melanogaster* ovarian egg chamber consists of 15 nurse cells and 1 oocyte that surrounded by a monolayer of somatic follicle cells [30]. Oogenesis in *Drosophila* can be divided into 14 morphologically distinct stages [31]. Throughout these stages, the oocyte remains transcriptionally quiescent [32] and depends heavily on nurse cells for the supply of critical components such as mRNAs [33], proteins, and organelles [34], which are delivered through specialized cytoplasmic bridges known as ring canals. This dynamic intracellular transport system facilitates the exchange of essential materials and makes the *Drosophila* ovary an ideal model for studying the mechanisms of membraneless organelle trafficking.

In all eukaryotic cells, the two fundamental cytoskeletal components are microtubules and microfilaments (F-actin) [35]. They are critical for cell division, cell migration, cargo transport and polarity establishment [36–39]. Microtubule based transport is mediated primarily by two types of motor proteins (kinesins and dynein), which move toward the microtubule's plus and minus ends, respectively, according to their intrinsic polarity [40–43]. Kinesin family motors generally transport cargoes toward the microtubule plus-end [44], while cytoplasmic dynein moves toward the minus-end [45]. The actin based motility, by contrast, is driven predominantly by myosin motor proteins that move along microfilaments [46].

To elucidate the trafficking mechanisms linking cytoophidia and the cytoskeleton, several studies have demonstrated that cytoophidia can interact closely with specific cytoskeletal components [47]. In the fission yeast *S. pombe*, for instance, the transport of CTPS cytoophidia during cytokinesis is driven by microfilaments and myosin, rather than microtubules [19]. Similarly, a systematic study in *Drosophila* revealed that multiple actin associated proteins are enriched through proximity labeling of cytoophidium, suggesting potential interactions between cytoophidia and microfilaments [47]. Despite these insights, it remains unclear whether the dynamics of cytoophidia are conserved in multicellular organisms, not to mention other possible regulatory mechanisms that have yet to be identified.

In this study, we utilize live-cell imaging to investigate the dynamic behavior of cytoophidia in *Drosophila* ovaries under physiological conditions. Our real-time imaging data reveal that the cytoskeleton, particularly microtubules, play a pivotal role in regulating cytoophidium dynamics. In control samples, cytoophidia exhibit robust motility, including active directional transport from nurse cells to oocytes. However, upon disruption of microtubules, we observe a significant reduction in cytoophidium movement and a loss of oocyte-directed trafficking, suggesting an essential requirement for the microtubule network in cytoophidium assembly and transport.

Materials and methods

Fly stocks

All flies used in this study were maintained at 25 °C and fed a corn-agar mixture. The fly stocks used in this research are as follows: C-terminal mCherry-4xV5 tagged CTPS knock-in flies (w^{1118} background) were generated in our laboratory. The stocks used were: Sp/Cyo; Sb/Tm6B (Core Facility of Drosophila Resource and Technology, CEMCS, CAS).

In this study, the Gal4/UAS system was utilized to achieve germline cell specific knockdown of the target gene in the fly ovary [48]. The stocks used were: *UAS-Khc- RNAi* (Tsinghua Fly Center # 1728); *Sp/Cyo; GFP-Pav /Tm6C.Sb* (Bloomington *Drosophila* Stock Center # 81651); *Nos-GAL4/Cyo;* $CTPS^{mCherry-KI}$*/Tm6C.Sb* (generated in this study).

Quantitative RT-PCR

Five to six pairs of *Drosophila* ovaries were collected from control and treatment groups, respectively. Total RNA was extracted using the TransZol Up Plus RNA Kit (TransGen Biotech). RNA concentration was measured, and 1 μg of total RNA was reverse transcribed into cDNA

with the ABScript III RT Master Mix for qPCR with gDNA Remover (ABclonal). Quantitative PCR was then performed using the resulting cDNA as template with 2X Universal SYBR Green Fast qPCR Mix (ABclonal) Reactions run in 96-well qPCR Plates (ABclonal) on a QuantStudio™ 7 Flex Real-Time PCR System (Applied BioSystems) to determine target RNA expression levels. We employed *rp49* as an internal reference gene for normalization. The corresponding primers were:

rp49 sense 5'- TACAGGCCCAAGATCGTGAA-3', antisense 5'- TCTCCTTGCGCTTCTTGGA-3'.

CTPS sense 5'-GAGTGATTGCCTCCTCGTTC-3', antisense 5'-TCCAAAAACCGTTCATAGTT-3'.

khc sense 5'- TGGAGGATCTCATGGAGGCA-3', antisense 5'- ATGCGCTTCTTCTGGTGTGA-3'.

Gal4 sense 5'- CAACTGGGAGTGTCGCTACTC –3', antisense 5'- CACCGTACTCGTCAATTCCAAG-3'.

Inhibitor treatment

Briefly, 2–4 day female files raised at 25 °C on a standard corn-meal agar, then these flies were fed with yeast paste supplemented with 200 μg/ml colchicine [49] (Adamas, 013456239) for 24 h to disrupt tubulin, or paclitaxel 250μM for 24 h to Stabilize microtubule structure [50]. Flies were fed with yeast paste supplemented with Cytochalasin D 500 μM for 24 h to disrupt microfilament [51] , or para-nitroblebbistatin 500 μM for 24 h to inhibit myosin [52]. To inhibit dynein flies were fed with yeast paste supplemented with 200μM Ciliobrevin D for 24 h [53]. Considering the differences in treatment methods and model organisms, we adjusted the drug concentrations in our experiments based on existing literature.

Immunofluorescence assay

This study on cytoophidia primarily focuses on stages 8-9 of the egg chamber. Ovaries were dissected from 2 to 5 days old female flies that had been supplemented with wet yeast two days before. After inducing CO_2 anesthesia, the dissection was performed using a stereomicroscope (Olympus SZ61) in a cell culture dish (Thermo Fisher Scientific, 150460) containing 3 ml of Grace's Insect Medium (Thermo Fisher Scientific, 11605094). The dissection was completed within 20 min to preserve the internal physiological structure of the ovaries. After removing the medium, the ovaries were fixed in 4% paraformaldehyde (PFA) (Alfa Aesar, 043368.9L) diluted in 1x PBS (MeilunBio, MA0015_500ML) for 10 min at room temperature. Following fixation, the ovaries underwent two rapid washes with PST (0.5% horse serum (Sunrise, SU1012) and 0.3% Triton X-100 (Thermo Fisher Scientific, 215682500) in 1x PBS) to eliminate any residual PFA. Next, 2 ml of PST was added, and any excess non-ovarian tissue was gently removed. The sample was then stored in PST and blocked for at least 2 h before immunofluorescence staining.

Before staining, 2-5 ovaries were washed once with PBST (0.3% Triton in PBS). The samples were first subjected to overnight incubation with primary antibodies at room temperature, followed by washes with PBST. Subsequently, they underwent a second overnight incubation with secondary antibodies at room temperature. We used rabbit anti-CTPS (1:1000; y-88, sc-134457, Santa Cruz Bio Tech Ltd.) to label CTPS cytoophidia. anti-rabbit with Cy5 (Jackson Immuno Research Laboratories, 711-175-152) was used as a secondary antibody. Hoechst 33342 (Bio-Rad, 1351304) specifically labels nuclei due to its high affinity for binding to DNA, and Rhodamine-conjugated phalloidin (1:200; SB-YP0059-50T, share-bio) was used to label the cell boundary by binding to F-actin.

Adult female flies at 2-5-day old pre-fed with wet yeast for two days, were dissected in phosphate-buffered saline (PBS). The isolated ovaries were then fixed for 20 min at 4 °C on a rocking platform in a solution containing 1× Brinkley Renaturing Buffer 80 (BRB80, pH 6.8), 0.1% Triton X-100, and 8% paraformaldehyde (PFA). The BRB80 formulation consisted of 80 mM piperazine-N, N′-bis (2-ethanesulfonic acid) (PIPES) (MCE, HY-W011271-10g), 1 mM $MgCl_2$ (Energy Chemical, A04012315-1kg), and 1 mM EGTA (Macklin, E762232-25ml). Upon completion of fixation, the sample was washed five times with PBTB (0.1% Triton X-100 + 0.2% BSA (Yeason, 36104ES25) in 1× PBS). Subsequently, samples were incubated overnight at 4 °C with a FITC-conjugated β-tubulin antibody (ProteinTech, Cat# CL488-66240) at a dilution of 1:100. The ovary was stained with CellMask Green Actin Tracking Stain (Cat. No. A57243) at 1X concentration for 30 min at 37℃.

Live imaging of *Drosophila* egg chamber

Dissect *Drosophila* ovaries in Schneider's *Drosophila* Medium (Thermo Fisher Scientific, 21720024) supplemented with 15% fetal bovine serum (FBS) (Yeason, 36104ES25), 0.2 mg/ml insulin (Yeason, 40112ES25), and 0.6× penicillin-streptomycin (PS) (Yeason, 60162ES76). Using tweezers, gently isolate individual ovarioles. Then, gather the isolated stage 8–9 egg chambers using an eyelash brush and transfer them with a pipette into 35 mm glass-bottom dishes (Cellvis, D35-10-1-N). Aspirate the medium, add 0.8% Agarose, Low melting (BBI, A600015-0005) dissolved in Schneider's *Drosophila* Medium (pre-dissolved at 65 °C), and allow it to dry at room temperature for approximately 10 min before proceeding with live-cell imaging.

Microscopy and image analysis

All images in this study were captured using laser-scanning confocal microscopy (Leica SP8 STED 3X)

and a Nikon Ti2-E + CSU W1 Sora 1 camera. Z-stacks were obtained for each egg chamber at intervals of 0.35 micrometers.

FIJI-ImageJ was used to analyze the length of cytoophidia. We used Fiji-ImageJ cell counter to calculate the number of cytoophidia. We used the Fiji-ImageJ Manual Tracking plugin to track the movement of cytoophidia. For each statistical quantification. The fluorescence intensity of cytoophidia in the egg chamber was measured using ImageJ. All measurements were performed on samples normalized for laser power and z-axis thickness during image acquisition.

Western blotting

The PVDF membrane was washed three times with TBST (Absin, abs952-1L) (5 min per wash), using a shaker at room temperature to remove excess blocking solution. It was then incubated with the following primary antibodies: anti-mCherry tag monoclonal antibody (Abbkine, A02080) to label CTPS, and anti-GAPDH monoclonal antibody (Novus, NB300-221SS) as the internal control. Then the membrane was washed three times with TBST (5 min per wash) on a shaker to remove excess primary antibody. Subsequently, the membrane was then transferred to the secondary antibody (Cell Signalling, anti-mouse IgG, HRP-linked antibody, 7076S) and incubated for 1 h at room temperature with shaking. After another three TBST washes (5 min each) to minimize background, the membrane was incubated with the Pierce ECL Reagent Kit (Thermo Fisher Scientific, 32106). The signal was then captured and documented using the Amersham Imager 600 (General Electric).

Protein expression was quantified by densitometry using ImageJ (National Institutes of Health, Bethesda, MD, USA) and internally standardized to GAPDH. Quantification was based on data collected from no fewer than three biological replicates.

Data analysis

Data presentation and statistical analysis: Results are reported as the mean ± SEM derived from a minimum of three independent biological replicates. The statistical comparison between groups utilized an unpaired two-tailed Student's t-test (GraphPad Prism 8.0). $P < 0.05$ was adopted as the threshold for statistical significance. Image and quantitative data processing: Confocal microscopy images were processed using ImageJ and Adobe Illustrator. All quantitative data analysis was executed using Excel and GraphPad software.

Results

Cytoophidia exhibit three distinct modes of dynamic behavior

To investigate the dynamic properties of cytoophidia, we performed live-cell imaging in *Drosophila* ovaries using a CTPS-mCherry fusion strain. Our analysis revealed that cytoophidia display three primary types of dynamic behavior within follicle cells and germline cells (including both oocytes and nurse cells): intracellular transport, intercellular movement, and morphological remodeling (Fig. 1; **Video S1**).

Within follicle cells, cytoophidia typically maintain a rigid and linear morphology. Trajectory analyses demonstrated that these cytoophidia exhibit bidirectional, back and forth motility along the apical-basal axis, suggesting a relatively constrained movement pattern (Fig. 1D). In contrast, cytoophidia in germline cells (oocytes and nurse cells) show more dynamic and less constrained movements (Fig. 1C). This increased mobility may facilitate interactions among cytoophidia, potentially contributing to their assembly.

Moreover, cytoophidia in germline cells frequently undergo active morphological remodeling, including processes such as twisting, flipping, and bending, often occurring concurrently with their movement. These structural changes further highlight the dynamic nature of cytoophidia in the germline and suggest a high degree of structural plasticity during their intracellular behavior (Figs. 1A, C).

To specifically visualize the intercellular transport of cytoophidia between nurse cells and oocytes, we employed GFP-Pav to label the ring canals. (Fig. 1A). Time-lapse imaging clearly captured instances of direct cytoophidium transport through ring canals, not only from nurse cells to oocytes but also between adjacent nurse cells (Figs. 1A, B). Given that the oocyte development relies heavily on nurse cells for the supply of essential biomolecules [28], this intercellular trafficking likely plays a critical role in oocyte development. Accordingly, we hypothesize that the directed movement of cytoophidia through ring canals may contribute to the delivery of functional components that support oocyte maturation.

Microtubules disassembly impairs Cytoophidium dynamics and assembly

In eukaryotic cells, intracellular transport is primarily mediated by motor proteins that move along microtubules and microfilaments [54]. Previous studies have demonstrated colocalization of cytoophidia and microtubules in follicular cells [2], so we first disrupted microtubule networks by treating adult flies with colchicine. The efficacy of microtubule depolymerization was assessed by immunofluorescence. Compared to the control group,

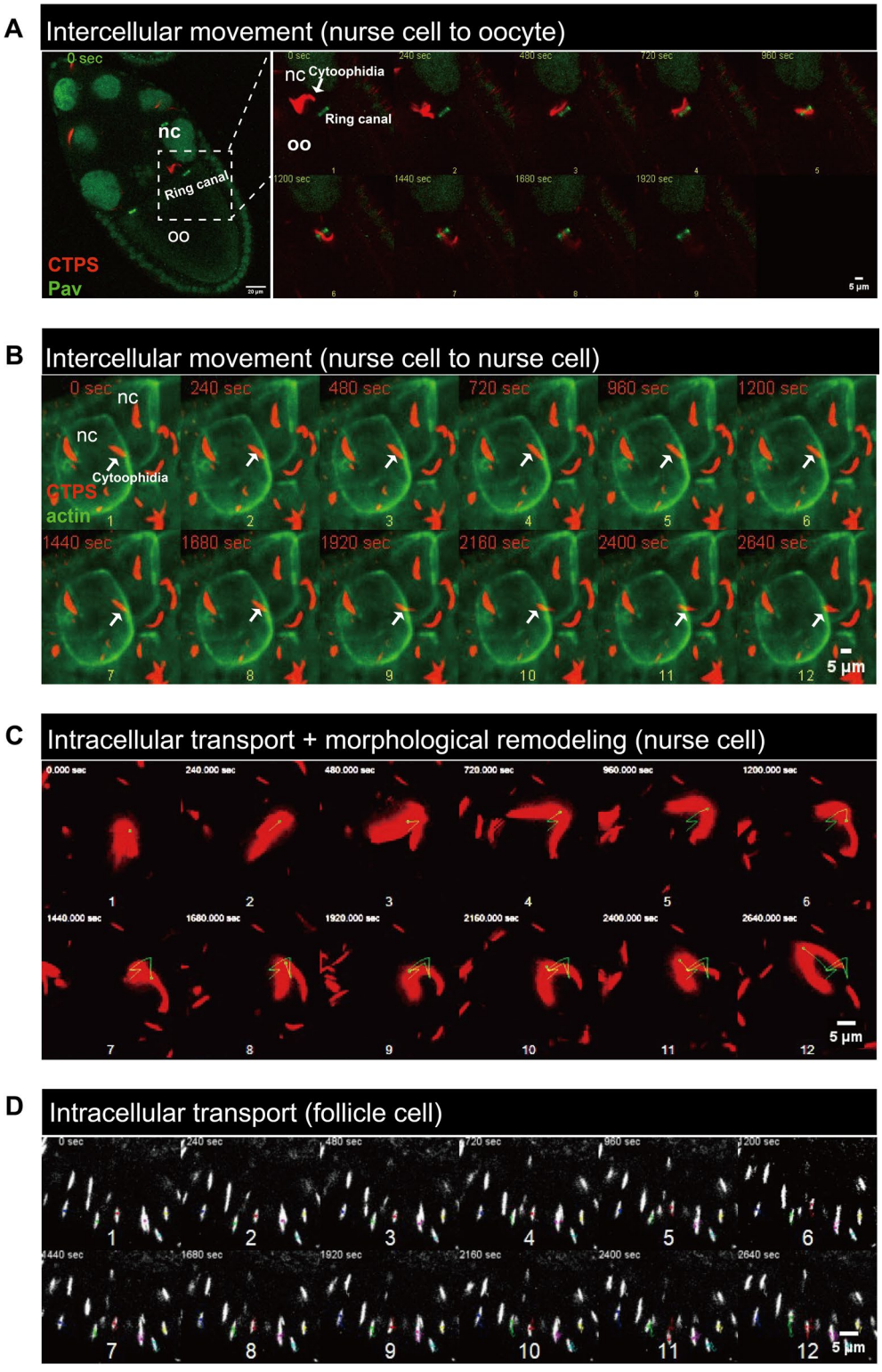

Fig. 1 Three types of dynamic changes in cytoophidia. **A** Live-cell imaging of cytoophidium (arrow) transporting from nurse cell (nc) to oocyte (oo). CTPS is tagged with mCherry (red), ring canal is labeled by GFP-Pav (green). Time stamps are on the top-left, images are taken for every 4 min. Scale bar, 20 μm (left), 5 μm (right). **B** Live-cell imaging of cytoophidium (arrow) transporting from one nurse cell to the other nurse cell. CTPS is tagged with mCherry (red), actin labeled by CellMask Green Actin Tracking Stain (green). Time stamps are on the top-left, images are taken for every 4 min. Scale bar, 5 μm. **C** Trajectories of cytoophidia in germline cells. CTPS is tagged with mCherry (red). Time stamps are on the top-left, images are taken for every 4 min. Time stamps are on the top-left, images are taken for every 4 min. Scale bar, 5 μm. **D** Trajectories of cytoophidia in follicle cells. CTPS is tagged with mCherry (gray). Time stamps are on the top-left, images are taken for every 4 min. Time stamps are on the top-left, images are taken for every 4 min. Scale bar, 5 μm.

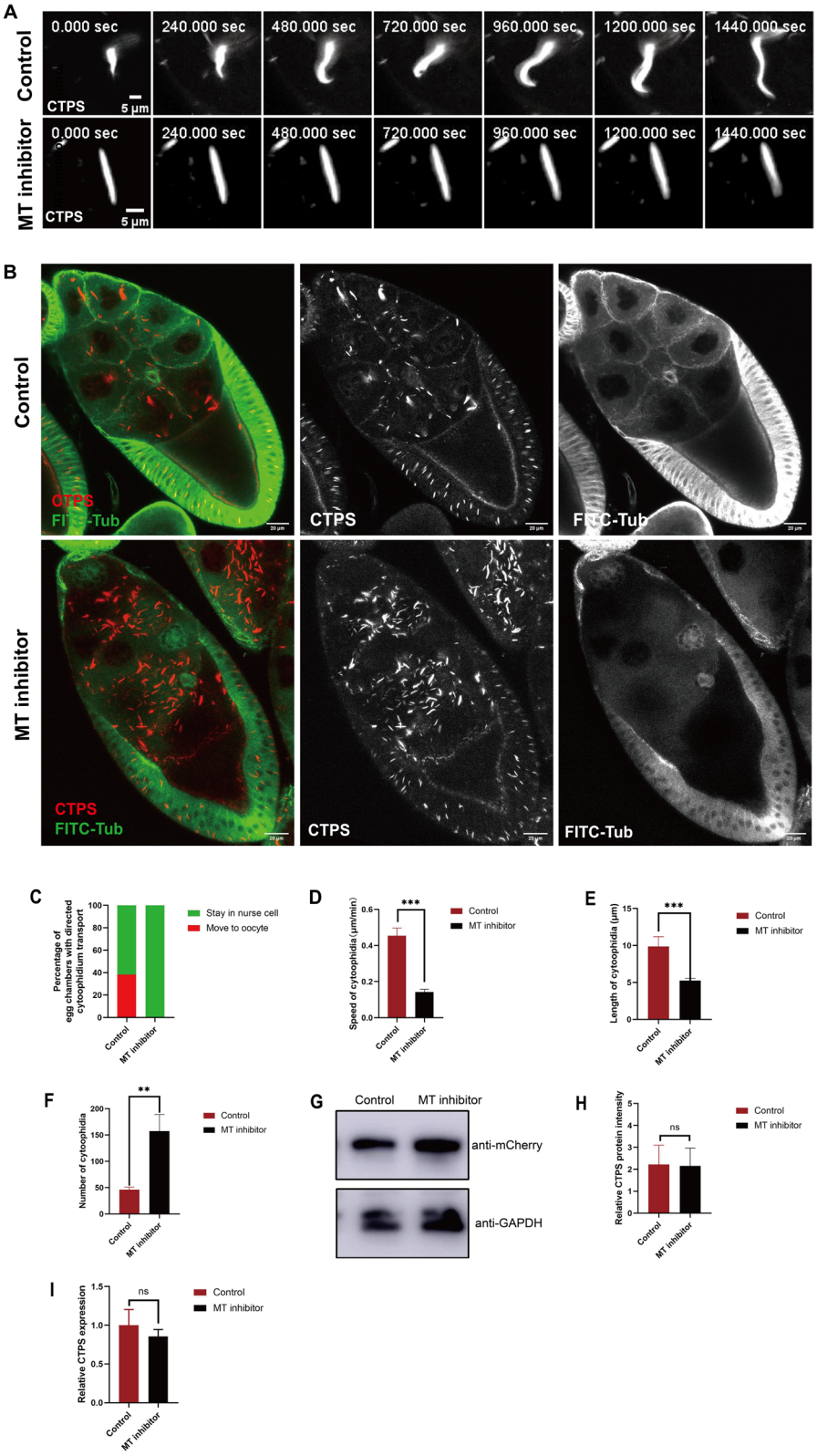

Fig. 2 (See legend on next page.)

(See figure on previous page.)

Fig. 2 Microtubules are essential for cytoophidium morphological changes, movement and assembly. **A** Time-lapse imaging revealed cytoophidia morphological changes, The time marked in the upper left corner represents the time since the capture began. The CTPS (gray) signal shown is obtained using mCherry-tagged CTPS. Scale bar = 5 μm. **B** Cytoophidia abundance and length are affected by microtubule depolymerization. Microtubules (green) are labeled with FITC-conjugated tubulin antibody. CTPS (red) signal is obtained using mCherry-tagged CTPS. scale bars, 20 μm. **C** Quantification of cytoophidium intercellular transportation through nurse cell-oocyte ring canals in control and microtubule inhibited groups. We analyzed 25 ovaries in control group and 25 ovaries in microtubule depolymerization group. **D** The speed of cytoophidia movement. We analyzed 35 filaments in control group and 35 filaments in microtubule depolymerization group. Data are represented as mean ± SEM. ***$p < 0.001$. **E** Length of cytoophidia in ovary nurse cell. We analyzed 32 filaments in control group and 88 filaments in microtubule depolymerization. Data are represented as mean ± SEM. ***$p < 0.001$. **F** Number of cytoophidia in ovary nurse cell. We analyzed 9 ovaries in control group and 413 filaments in total, and 9 ovaries in microtubule depolymerization and 1417 filaments in total, Data are represented as mean ± SEM. **$p < 0.001$. **G** Western blotting analysis of CTPS proteins from ovary of CTPS-mCherry fly. Anti-mCherry antibody was used for the immunoblotting analysis. GAPDH was used as an internal control. **H** The CTPS protein levels in the samples from **G** were quantified. Data are represented as mean ± SEM. ns, no significance in difference. **I** Measurement of the relative CTPS mRNA expression was conducted *via* quantitative RT-PCR using ovary from the control and MT inhibitor-treated flies (6 ovaries/group, 3 biological replicates). Data are represented as mean ± SEM. ns, no significance in difference

colchicine treatment resulted in a marked disruption of the microtubule cytoskeleton, with barely detectable intact microtubule signals in treated samples (Fig. 2B).

Coincident with microtubule loss, we observed a striking stabilization of cytoophidium morphology. Instead of exhibiting the dynamic shape shifting behavior seen in control cells, cytoophidia in colchicine-treated samples displayed a static, unchanging structure (Fig. 2A; **Video S2**). This indicates that intact microtubules are required to sustain the dynamic morphological transitions of cytoophidia.

To further characterize the impact of microtubule disruption on cytoophidium motility, we analyzed their movement trajectories. Strikingly, microtubule depolymerization led to a severe suppression of cytoophidium dynamics, with significantly reduced motility (Figs. 2D; **Video S2**). More importantly, directed transport of cytoophidia from nurse cells to the oocyte *via* ring canals was completely abolished (Fig. 2C). This finding strongly suggests that functional microtubule networks are essential for the directional, intercellular movement of cytoophidia.

In addition to impaired motility, microtubule disruption also had a notable impact on cytoophidium assembly. Quantitative analysis demonstrated a striking increase in the number of cytoophidia which accompanied by shorter filament (Fig. 2B, E and F). To preclude the possibility that the observed increase was merely a consequence of elevated CTPS expression, we performed quantitative PCR (qPCR) and Western blotting to measure CTPS transcript and protein levels, respectively. Importantly, neither CTPS mRNA nor protein abundance was significantly altered following colchicine treatment (Fig. 2G, H and I). These results indicate that microtubules regulate cytoophidium assembly independently of changes in CTPS expression levels.

Taken together, these findings demonstrate that microtubules play a central role in multiple aspects of cytoophidium including morphological dynamics, intracellular and intercellular motility, and the assembly process.

Stabilization of microtubules does not significantly alter Cytoophidium dynamics or assembly

Having established that microtubule disassembly disrupts cytoophidium dynamics and impairs their assembly, we next sought to investigate whether microtubule stabilization similarly influences these processes. To this end, we treated adult *Drosophila* with the microtubule-stabilizing agent paclitaxel.

Immunofluorescence analysis revealed after being treated with paclitaxel, the fluorescence intensity is significantly increase compared to untreated controls (Fig. 3B). This pharmacological effect confirms the effectiveness of paclitaxel in inducing stable microtubule networks in our experimental system.

To assess the impact of microtubule stabilization on cytoophidium behavior, we performed live-cell imaging under physiological conditions. Strikingly, cytoophidia in paclitaxel treated flies retained their characteristic morphological plasticity, exhibiting a range of dynamic behaviors similar to those observed in control samples (Fig. 3A; **Video S3**). Individual cytoophidium structures continued to display heterogeneous motility patterns, and key intrinsic motility parameters including speed and directional persistence remained largely unchanged (Fig. 3C and D; **Video S3**).

Quantitative analysis further demonstrated that neither the number nor the mean filament length of cytoophidia was statistically significantly changed in the paclitaxel-treated group compared to the control (Fig. 3E and F). In addition, the result shows no evident difference in CTPS signal intensity between control and paclitaxel treated cells (Fig. 3G).

These findings suggest that microtubule stabilization does not overtly enhance or inhibit the dynamic assembly or maintenance of cytoophidia. Taken together, our results indicate that while microtubule disassembly disrupts cytoophidium dynamics and assembly, microtubule stabilization alone is insufficient to modulate these processes. We therefore speculate that cytoophidium assembly and dynamics may depend more critically on the polymerization state.

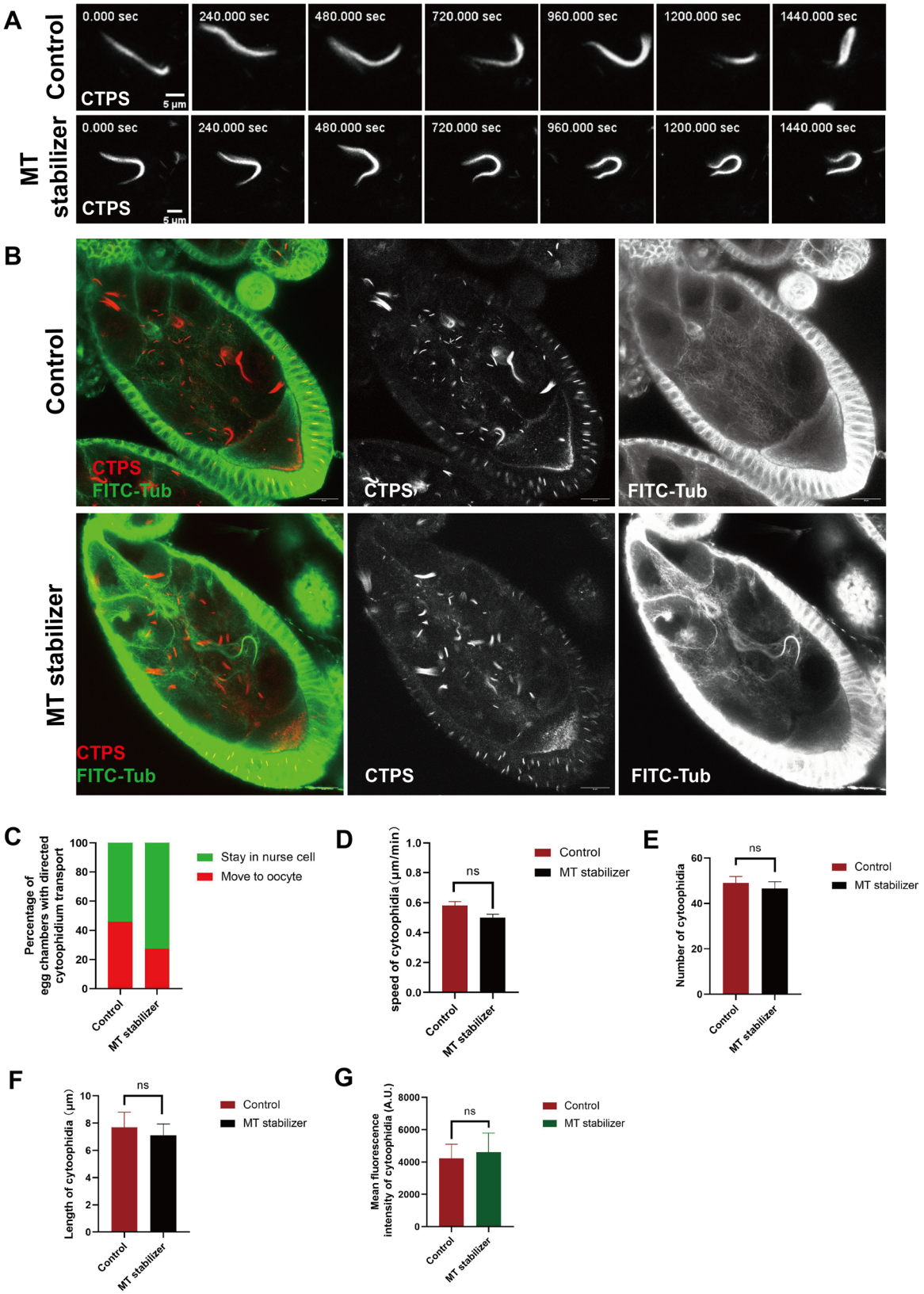

Fig. 3 (See legend on next page.)

(See figure on previous page.)

Fig. 3 Microtubules stabilization does not affect cytoophidium morphological changes, movement and assembly. **A** Time-lapse imaging revealed cytoophidia morphological changes, The time marked in the upper left corner represents the time since the capture began. The CTPS (gray) signal shown is obtained using mCherry-tagged CTPS. Scale bar = 5 μm. **B** Cytoophidia abundance and length are not affected by microtubule polymerization. Microtubules (green) are labeled with FITC-conjugated tubulin antibody. CTPS (red) signal is obtained using mCherry-tagged CTPS. scale bars, 20 μm. **C** Quantification of cytoophidia transport through nurse cell-oocyte ring canals in control and microtubules polymerization groups. We analyzed 14 ovaries in control group and 14 ovaries in microtubule polymerization group. **D** The speed of cytoophidia movement. We analyzed 47 filaments in control group and 47 filaments in microtubule polymerization group. Data are represented as mean ± SEM. ns, no significance in difference. **E** Number of cytoophidia in ovary nurse cell. We analyzed 5 ovaries in control group and 245 filaments in total, and 5 ovaries in microtubule polymerization and 233 filaments in total. Data are represented as mean ± SEM. ns, no significance in difference. **F** Length of cytoophidia in ovary nurse cell. We analyzed 47 filaments in control group and 47 filaments in microtubule polymerization. Data are represented as mean ± SEM. ns, no significance in difference. **G** Intensity of CTPS-mCherry fluorescence signal in cytoophidia (ns, no significance in difference). 3 ovaries in control group and 3 ovaries in MT stabilizer-treated group are analyzed. Data are represented as mean ± SEM.

Cytoplasmic dynein drives the directed trafficking of cytoophidia

Given that microtubules are essential for the directed transport and dynamics of cytoophidia, we next sought to identify the specific motor proteins responsible for mediating this process. Among the known microtubule based motor proteins, Cytoplasmic dynein is a motor protein that moves toward the minus end of microtubules and plays a central role in the intracellular transport of various membranous and membraneless cargoes, including peroxisomes, autophagosomes, lipid droplets, and mitochondria [55]. Given that cytoophidia are membraneless organelles that undergo directed transport from nurse cells to oocytes through ring canals, we hypothesized that dynein may also be involved in their long range, directional motility.

To test this hypothesis, we inhibited dynein activity using ciliobrevin D, a small-molecule inhibitor that specifically blocks cytoplasmic dynein function [53], and examined its effects on cytoophidium behavior. Live imaging analysis revealed that dynein inhibition did not significantly affect cytoophidium morphology (Fig. 4A). Moreover, both the dynamic behaviors and movement trajectories of cytoophidia remained largely unchanged in the presence of ciliobrevin D (Fig. 4C; **Video S4**). Interestingly, the proportion of directed transport events from nurse cells to oocytes through ring canals was significantly decreased (Fig. 4B). These observations suggest that dynein is dispensable for the maintenance of general motility or morphological plasticity of cytoophidia under these conditions.

However, quantitative analysis of cytoophidium populations revealed significant changes in their size distribution. Specifically, we observed a marked increase in the proportion of shorter cytoophidium fragments in dynein inhibited samples compared to controls (Fig. 4D and E). Notably, this alteration in cytoophidium length distribution was not accompanied by significant changes in CTPS mRNA (Fig. 4F). Furthermore, CTPS-mCherry fluorescence signal intensity revealed no significant change between control and dynein inhibited group cells (Fig. 4G), suggesting that the effect is unlikely to result from altered transcription or translation of CTPS. Instead, these data point to a potential role for dynein in regulating cytoophidium assembly or fragment stability. Collectively, these results demonstrate that dynein inhibition leads to changes in cytoophidium size and directed transport from nurse cell to oocyte, while not impairing their overall morphology and motility.

Kinesin plays a limited role in the regulation of Cytoophidium dynamics

Kinesin is a plus end directed microtubule motor protein that functions as a tetrameric complex, composed of two heavy and two light chains [56]. Through its ATP dependent conformational changes, kinesin generates mechanical force to transport various cellular cargoes toward the plus ends of microtubules [57]. Given its established role in intracellular transport, we hypothesized that kinesin might also contribute to the regulation of cytoophidium motility or transport.

To investigate this possibility, we examined cytoophidium behavior in genetic backgrounds where kinesin heavy chain (*Khc*) was knocked down *via* RNA interference (RNAi). Live-cell imaging revealed that cytoophidium morphological dynamics remained largely unaffected after *Khc* knockdown (Fig. 5A; **Video S5**). Specifically, time-lapse imaging consistently captured ongoing structural transformations of cytoophidia (Fig. 5A), indicating that their intrinsic plasticity and remodeling processes were preserved in the absence of *Khc*.

Further quantitative analysis of cytoophidium behaviors showed that kinesin inhibition did not disrupt their directional transport from nurse cells to oocytes *via* ring canals. (Fig. 5C). In addition, no statistically significant changes were observed in the motility rates of cytoophidia (Fig. 5D). Besides the proportion of disassembled cytoophidia within the egg chambers of *Khc* RNAi flies is also not changed (Fig. 5B, E and F). Quantitative analysis revealed no statistically significant difference in the cytoophidia fluorescence intensity between the *Khc* RNAi group and the control group (Fig. 5G). In summary, kinesin does not play a major role in the regulation of

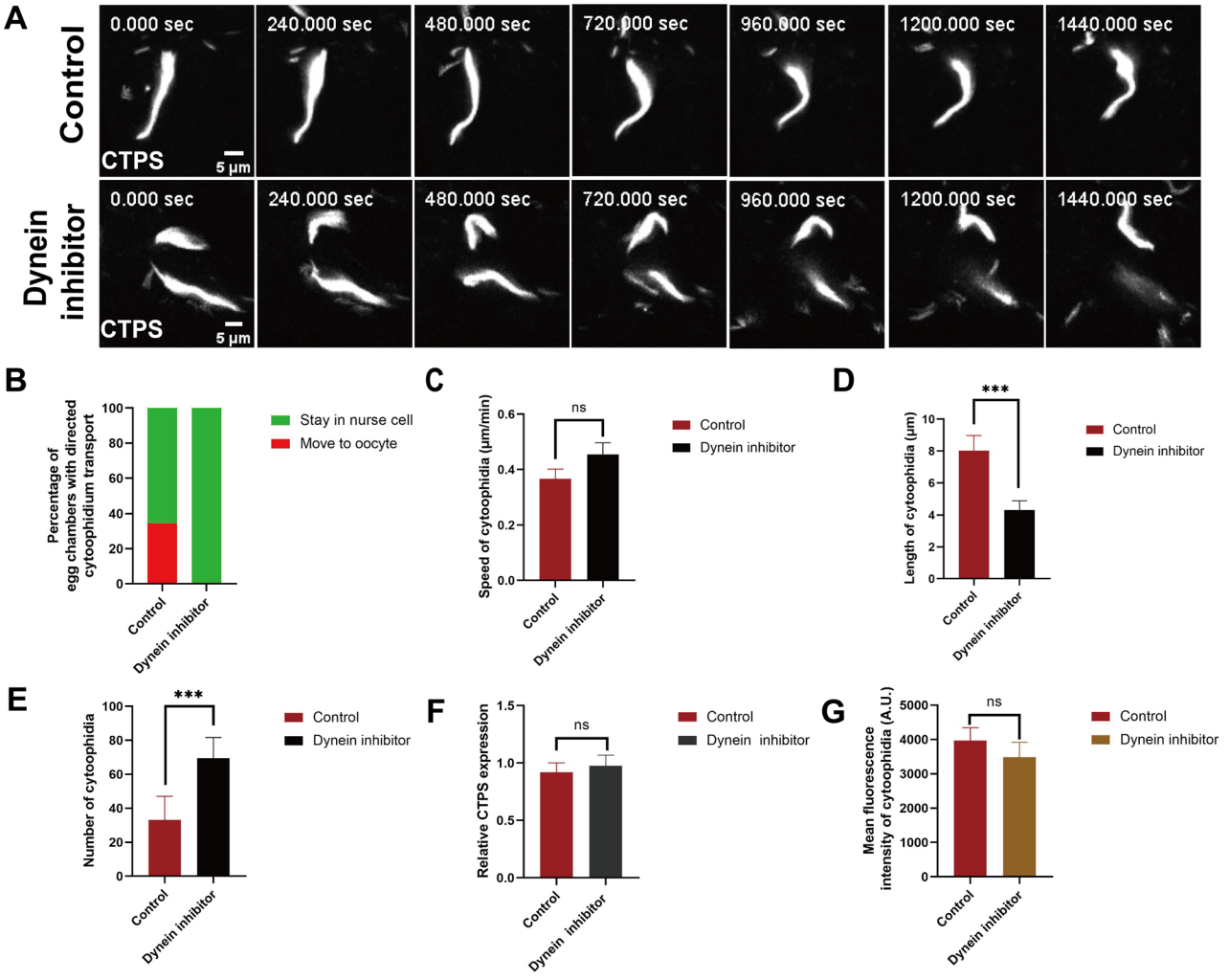

Fig. 4 Dynein is indispensable for assembly and directed movement of cytoophidia. **A** Time-lapse imaging revealed cytoophidia morphological changes, The time marked in the upper left corner represents the time since the capture began. The CTPS (gray) signal shown is obtained using mCherry-tagged CTPS. Scale bar = 5 μm. **B** Quantification of cytoophidia transport through nurse cell-oocyte ring canals in control and dynein inhibited groups. We analyzed 16 ovaries in control group and 18 ovaries in dynein inhibited group. **C** The speed of cytoophidia movement. We analyzed 35 filaments in control group and 35 filaments in dynein inhibited group. Data are represented as mean ± SEM. ns, no significance in difference. **D** Length of cytoophidia in ovary nurse cell. We analyzed 43 filaments in control group and 47 filaments in dynein inhibited. Data are represented as mean ± SEM. ***$p < 0.001$. **E** Number of cytoophidia in ovary nurse cell. We analyzed 8 ovaries in control group and 265 filaments in total, and 8 ovaries in dynein inhibited and 557 filaments in total. Data are represented as mean ± SD. ****$p < 0.0001$. **F** Quantitative RT-PCR was used to assess the relative expression levels of CTPS mRNA. Ovaries were collected from the control and dynein inhibitor-treated flies (6 ovaries/group, 3 biological replicates). Data are represented as mean ± SEM. ns, no significance in difference. **G** Intensity of CTPS-mCherry signal in cytoophidia (ns, no significance in difference). 3 ovaries in control group and 3 ovaries in dynein inhibited group are analyzed. Data are represented as mean ± SEM.

cytoophidium motility, transport, or structural stability under physiological conditions.

The dynamics and assembly of cytoophidia depend on microfilaments

Microfilament is a key component of the cytoskeletal network, which plays essential roles across a variety of cellular processes, including intracellular transport, cell motility, and the maintenance of cellular architecture [58]. Previous studies in the fission yeast *Schizosaccharomyces pombe* have suggested that microfilaments regulate cytoophidium dynamics through the modulation of filament aggregation [19], highlighting a potential conserved role in cytoophidium regulation. To investigate whether this function is evolutionarily conserved in multicellular organisms, we examined the effects of microfilament disruption on cytoophidium behavior in *Drosophila* ovaries.

We treated adult flies with cytochalasin D, a potent inhibitor of actin polymerization [51], and analyzed the resulting effects on cytoophidium dynamics and assembly. Live-cell imaging revealed that microfilament disruption significantly impaired the dynamic behavior of

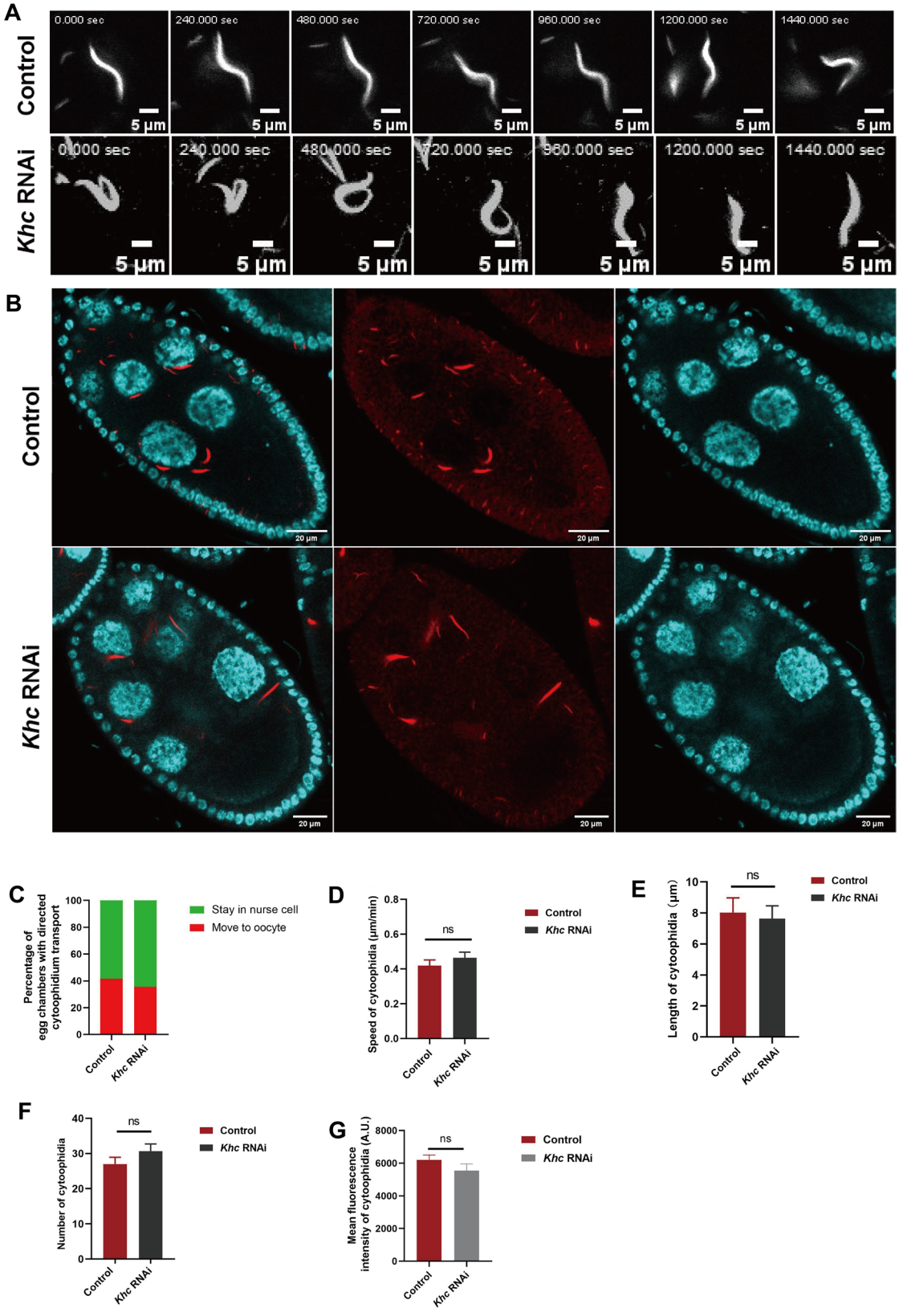

Fig. 5 (See legend on next page.)

(See figure on previous page.)

Fig. 5 Kinesin does not affect cytoophidia dynamic changes. **A** Time-lapse imaging revealed cytoophidia morphological changes, The time marked in the upper left corner represents the time since the capture began. The CTPS (gray) signal shown is obtained using mCherry-tagged CTPS. Scale bar = 5 μm. **B***Khc* knockdown *Drosophila* ovaries. CTPS (red) signal shown is obtained using mCherry-tagged CTPS. Nuclei(blue) are stained by Hoechst 33342. scale bars, 20 μm. **C** Quantification of cytoophidia transport through nurse cell-oocyte ring canals in control and *Khc* knockdown groups. We analyzed 30 ovaries in control group and 25 ovaries in *Khc* knockdown group. **D** The speed of cytoophidia movement. We analyzed 41 filaments in control group and 30 filaments in *Khc* knockdown group, Data are represented as mean ± SEM. ns, no significance in difference. **E** Length of cytoophidia in ovary nurse cell. We analyzed 43 filaments in control group and 44 filaments in *Khc* knockdown, Data are represented as mean ± SEM. ns, no significance in difference. **F** Number of cytoophidia in nurse cell. We analyzed 6 ovaries in control group and 162 filaments in total, and 6 ovaries in *Khc* knockdown and 184 filaments in total, Data are represented as mean ± SEM. ns, no significance. **G** Intensity of CTPS-mCherry fluorescence signal in cytoophidia (ns, no significance in difference). 3 ovaries in control group and 3 ovaries in *Khc* group are analyzed. Data are represented as mean ± SEM.

cytoophidia (**Video S6**). Specifically, actin depolymerization arrested the morphological remodeling of cytoophidia, locking them into static, unchanging architectural states (Fig. 6A; **Video S6**). This phenotype closely resembled the effects of microtubule disruption, suggesting that both cytoskeletal systems are critical for maintaining the structural plasticity of cytoophidia.

In addition to impaired morphological dynamics, actin inhibition also led to the fragmentation of large cytoophidia into smaller, disassembled ones (Fig. 6B, E and F). Notably, quantitative analysis revealed a shift in cytoophidium size distribution toward smaller fragments, indicative of a loss of higher order assembly (Fig. 6B). Importantly, this structural disassembly occurred without significant changes in CTPS transcriptional expression, as determined by qPCR (Fig. 6G). Comparative analysis of ovary revealed that the fluorescence intensity of cytoophidia was statistically invariant in the actin inhibited group compared to the control group (Fig. 6H). These findings suggest that microfilaments are specifically required for maintaining the integrity and higher order assembly of cytoophidia, independent of CTPS and protein expression levels.

Furthermore, quantitative analysis of cytoophidium motility and transport behavior demonstrated that actin inhibition led to a dramatic reduction in their intracellular motility (Fig. 6D; **Video S6**). The frequency of directed transport events from nurse cells to oocytes was significantly decreased (Fig. 6C). These results indicate that microfilaments play a critical role in mediating the intercellular trafficking of cytoophidia.

Taken together, these findings demonstrate that microfilaments are essential for both the dynamic remodeling and assembly of cytoophidia and are additionally required for their efficient intercellular transport in the *Drosophila* ovary. The phenotypic similarities between actin and microtubule disruption further suggest that cytoophidium dynamics rely on a coordinated interplay between multiple cytoskeletal systems.

Myosin II acts as a key motor protein in regulating Cytoophidium dynamics and assembly

Myosin is a superfamily of actin-based motor proteins that generate mechanical force through ATP dependent interaction with microfilaments, enabling the transport of cellular cargoes and the regulation of cytoskeletal dynamics [59]. Among them, myosin II is a key regulator of cellular contractility, motility, and the maintenance of cellular architecture, and is implicated in processes requiring dynamic remodeling of the actin cytoskeleton [60]. To investigate the potential role of myosin II in modulating cytoophidium dynamics, we treated *Drosophila* samples with para-nitroblebbistatin [52], a selective inhibitor of myosin II ATPase activity.

Our results demonstrated that inhibition of myosin II significantly suppressed the morphological dynamics of a subset of cytoophidia. The most notably reduction in their ability to undergo shape changes such as bending, twisting, or remodeling (Fig. 7A). This observation indicates that myosin II contributes to the structural plasticity and dynamic remodeling of cytoophidia, likely through its role in actin mediated cytoskeletal organization.

In addition to impaired morphological flexibility, myosin II inhibition also markedly reduced the overall motility of cytoophidia (Fig. 7C, **Video S7**). We observed a complete loss of intercellular directed transport of cytoophidia *via* ring canals (Fig. 7B). This finding highlights the essential role of myosin II in mediating the directed, intercellular movement of cytoophidia, a process critical for oocyte development.

Furthermore, quantitative analysis of cytoophidium size distribution revealed a significant increase in the abundance of small cytoophidia following myosin II inhibition. These smaller cytoophidia were statistically shorter in length compared to those observed in control samples (Fig. 7D and E). Since CTPS did not change at either the mRNA or protein level (Fig. 7F and G), suggests that myosin II is critically involved in the assembly of cytoophidium, rather than in the regulation of CTPS levels.

Taken together, these findings demonstrate that myosin II plays a multifaceted role in the regulation of cytoophidium biology. It is essential for their dynamic morphological remodeling, their intercellular transport, and their proper assembly into functional filamentous structures. These results further emphasize the coordinated action of multiple cytoskeletal motors, including

myosin II, dynein, and potentially others, in orchestrating the complex behavior of cytoophidia within the *Drosophila* ovary.

Discussion

Cytoskeletal control of Cytoophidium assembly and morphological plasticity

Our findings reveal that the cytoskeleton plays an essential and multifaceted role in regulating both the assembly and dynamic morphology of cytoophidia. Pharmacological disruption of microtubules using colchicine led to a marked reduction in large, filamentous cytoophidia and a concomitant increase in smaller cytoophidium fragments, implying a requirement for microtubules to maintain the assembly these membraneless organelles. Similarly, inhibition of microfilament polymerization with cytochalasin D resulted in a comparable phenotype, characterized by impaired morphological remodeling and the emergence of smaller cytoophidia. These observations indicate that both microtubules and microfilaments are critical for sustaining the structural stability and dynamic plasticity of cytoophidia, although their precise contributions may differ in mechanism or context.

These findings resonate with previous biochemical and structural studies of CTPS, the enzymatic core of cytoophidia, which polymerizes into filamentous assemblies both *in vivo* and *in vitro*. CTPS forms tetramers that serve as its basic functional units CTPS [61–63], and in *Drosophila*, these tetramers further assemble into filaments through interactions within the α-helix region of the GAT domain [64]. In parallel, recombinant *Escherichia coli* CTPS (ecCTPS) has been shown to form bundled filamentous structures under controlled conditions *in vitro* [3], supporting the idea that CTPS has an intrinsic propensity to assemble into higher order structures. However, the mechanisms by which these CTPS filaments or bundles mature into the light microscopy visible cytoophidia observed *in vivo* remain poorly understood.

Our data strongly support the hypothesis that the cytoskeleton, particularly microtubules and microfilaments mediate the transition from CTPS polymerization to functional cytoophidium assembly. This may occur through mechanisms active transport that facilitates aggregation. Nonetheless, the precise molecular determinants of cytoophidium assembly, including the signals and adaptors that link CTPS filaments to the cytoskeleton, as well as the rules governing their size, distribution, and coalescence, remain to be elucidated.

Cytoskeletal motors orchestrate Cytoophidium dynamics and directed transport

We demonstrate that dynein and myosin are essential for orchestrating the long range, directed transport of cytoophidia from nurse cells to the oocyte. Inhibition of either myosin or dynein disrupts the directed transport. These findings advance our understanding of the molecular mechanisms regulating cytoophidia dynamics.

While this study addresses the role of individual motor proteins in cytoophidium transport, the effects of motor–motor interactions on cytoophidium behavior remain poorly explored. Previous work has shown that *myo1c*, a non-processive single headed motor, can cooperate with microtubule based motors such as kinesin-1 [65]. Other studies have also indicated that dynein–kinesin coordination is required for polar transport in *Drosophila* oocytes [55]. Furthermore, dynein has been found to act synergistically with myosin II during cargo delivery through ring canals between cells [66]. Together, these observations suggest that cytoophidia dynamics may be regulated by multiple motor proteins acting in concert. However, it remains unclear whether individual motor proteins influence each other during cytoophidia transport, and the mechanistic basis underlying their coordinated action in this process awaits further elucidation. Subsequent investigations should employ specialized assays to address these important questions.

While dynein inhibition with ciliobrevin D abolished cytoophidium trafficking through ring canals, both morphological remodeling and intracellular movement were unaffected. This underscores that dynein is not broadly required for cytoophidium dynamics, while it is specifically dedicated to their directional intercellular transport, a process critical for oocyte maturation.

In vivo, dynein functions by assembling into a multiprotein transport complex composed of dynactin and specific adaptor proteins, which collectively mediate precise cargo recognition and processive movement along microtubules [67–69]. In *Drosophila* oogenesis, a highly conserved dynein-dynactin-based machinery, also involving Bicaudal D (*BicD*) and Egalitarian (*Egl*), drives the polarized transport of mRNP complexes, organelles, and proteins from nurse cells to the oocyte [70–73]. This system ensures that the transcriptionally silent oocyte receives essential developmental determinants *via* microtubule guided transport. As membraneless organelles, cytoophidia still have many key questions unresolved. For instance, how are cytoophidia selectively recognized and recruited by motors? What molecular or cellular cues trigger their dynamic remodeling, assembly, and transport?

Functional significance of Cytoophidium transport and dynamics in oogenesis

Beyond their structural role, the transport and dynamic behavior of cytoophidia likely serve important physiological functions in oogenesis. We propose that cytoophidium dynamics contribute to both metabolic enzyme

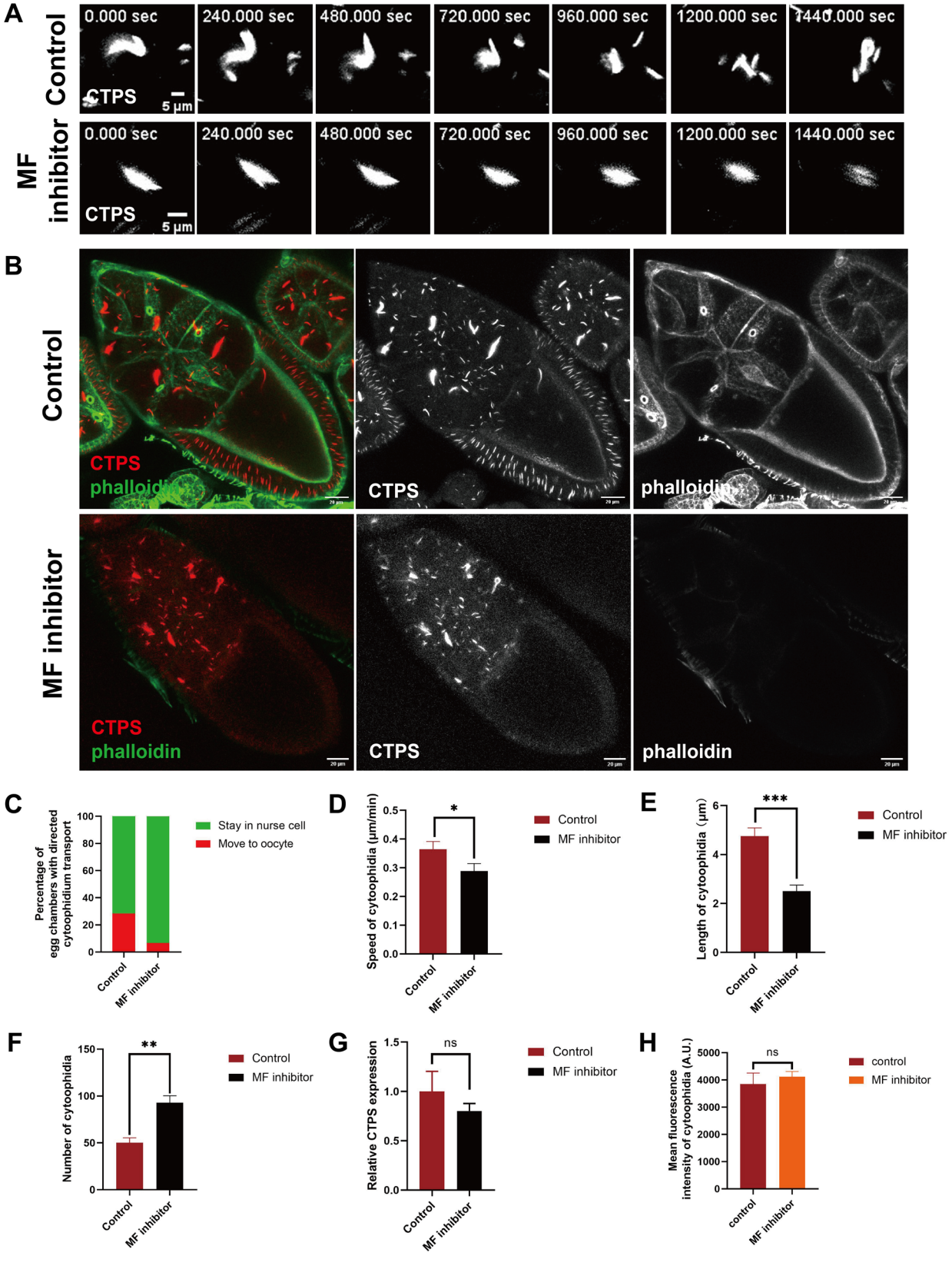

Fig. 6 (See legend on next page.)

(See figure on previous page.)

Fig. 6 Microfilaments are essential for movement, morphological changes and assembly of cytoophidia. **A** Time-lapse imaging revealed cytoophidia morphological changes, The time marked in the upper left corner represents the time since the capture began. The CTPS (gray)signal shown is obtained using mCherry-tagged CTPS. Scale bar = 5 μm. **B** Cytoophidia abundance and length are affected by microfilaments depolymerization. Microfilaments (green) are labeled with phalloidin, CTPS (red) signal shown is obtained using mCherry-tagged CTPS. scale bars, 20 μm. **C** Quantification of cytoophidia transport through nurse cell-oocyte ring canals in control and microfilaments depolymerization groups. We analyzed 27 ovaries in control group and 27 ovaries in microfilaments depolymerization group. **D** The speed of cytoophidia movement. We analyzed 48 filaments in control group and 48 filaments in microfilaments depolymerization group. Data are represented as mean ± SEM, $*p < 0.05$. **E** Length of cytoophidia in ovary nurse cell. We analyzed 184 filaments in control group and 184 filaments in microfilaments depolymerization. Data are represented as mean ± SEM, $***p < 0.001$. **F** Number of cytoophidia in ovary nurse cell. We analyzed 9 ovaries in control group and 450 filaments in total, and 9 ovaries in microfilaments depolymerization and 835 filaments in total. Data are represented as mean ± SEM, $**p < 0.01$. **G** The relative expression of CTPS mRNA was acquired and quantified utilizing quantitative PCR using ovary from the control and microfilaments inhibitor-treated flies (6 ovaries/group, 3 biological replicates). Data are represented as mean ± SEM, ns, no significance. **H** Intensity of CTPS-mCherry signal in cytoophidia (ns, no significance in difference). 3 ovaries in control group and 3 ovaries in microfilaments inhibited group are analyzed. Data are represented as mean ± SEM.

redistribution and intracellular homeostasis. By directed transport, the system may facilitate rapid, localized metabolic support, effectively acting as a buffer to stabilize CTPS concentrations and modulate metabolic flux in response to developmental events.

This model is consistent with previous studies showing that CTPS filamentation is responsive to cellular stress and linked to modulation of enzyme activity modulation [3]. Moreover, given that *Drosophila* oocytes are transcriptionally silent during growth and depend entirely on nurse cell derived mRNAs, proteins, and organelles for their development [74], the transport of cytoophidia *via* microtubule based motors is likely to be tightly integrated with oocyte metabolic regulation and developmental progression.

Thus, cytoophidium dynamics are not merely a reflection of passive CTPS polymer behavior, but are functionally coupled to the oocyte need for metabolic coordination, resource allocation, and intercellular communication. Future studies aimed at dissecting the molecular signals governing their transport will shed light on how these organelles contribute to oocyte maturation and reproductive success.

Conclusion

In summary, our study demonstrates that the cytoskeleton through the coordinated action of microtubules and microfilaments plays a central role in regulating the assembly, structural dynamics, and directional transport of cytoophidia in the *Drosophila* ovary (Fig. 8). We identified dynein and myosin as responsible for long range, intercellular cytoophidium trafficking. In addition, myosin II was shown to regulate their morphological plasticity and local assembly.

These findings highlight the remarkable complexity and specificity of cytoskeletal regulation in controlling the lifecycle of a membraneless organelle. They also provide a foundation for future investigations into the molecular mechanisms underlying cytoophidium recruitment, assembly, and transport, as well as their broader physiological roles in oogenesis and beyond.

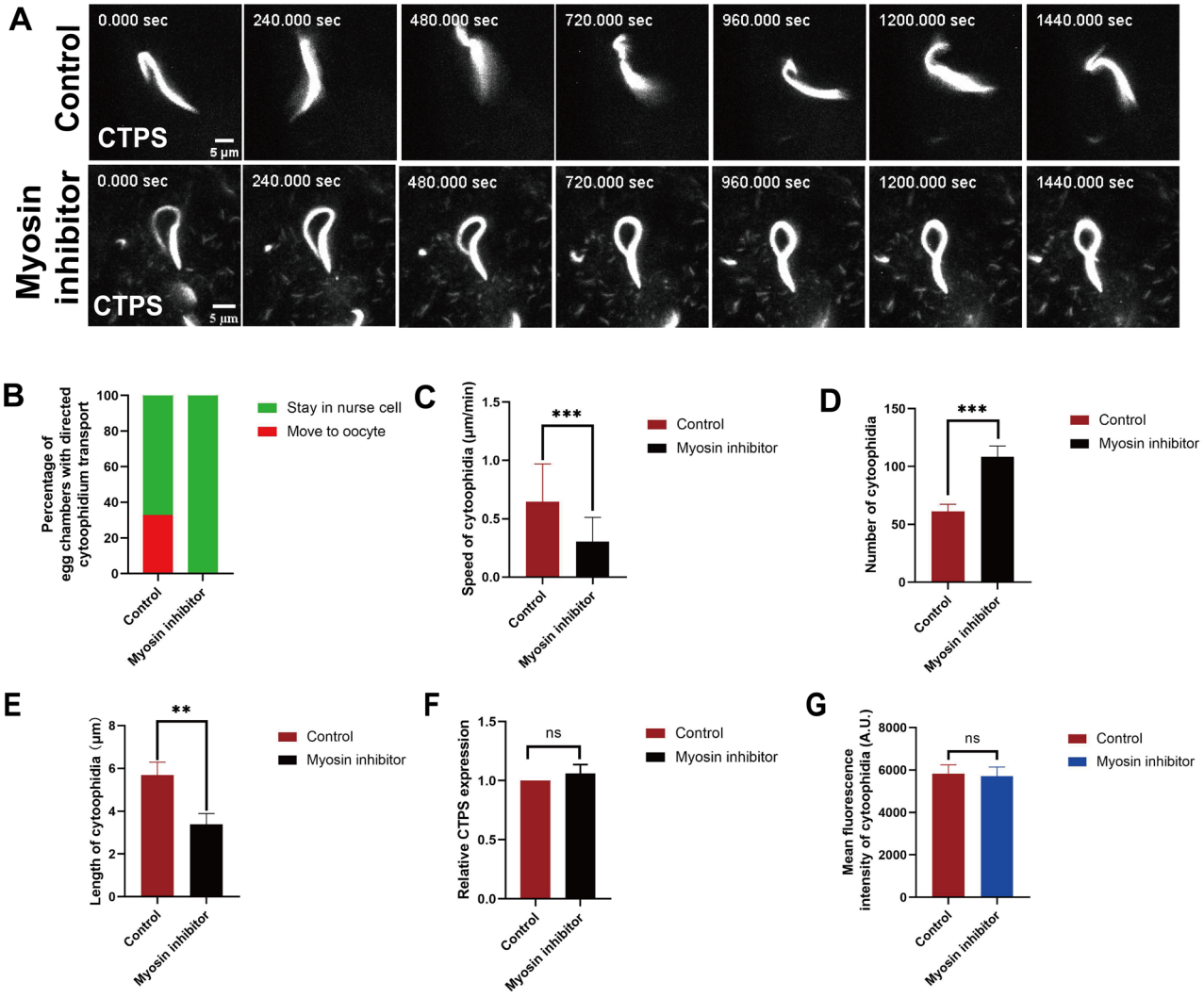

Fig. 7 Myosin is essential for movement, morphological changes and assembly of cytoophidia. **A** Time-lapse imaging revealed cytoophidia morphological changes, The time stamps represent the time since the capturing began. The CTPS (gray) signal shown is obtained using mCherry-tagged CTPS. Scale bar = 5 μm. **B** Quantification of cytoophidia transport through nurse cell-oocyte ring canals in control and myosin inhibited groups. We analyzed 19 ovaries in control group and 19 ovaries in myosin inhibited group. **C** The speed of cytoophidia movement. We analyzed 56 filaments in control group and 56 filaments in myosin inhibited group. Data are represented as mean ± SEM, ***$p < 0.001$. **D** Number of cytoophidia in ovary nurse cell. We analyzed 10 ovaries in control group and 581 filaments in total, and 10 ovaries in myosin inhibited and 989 filaments in total. Data are represented as mean ± SEM, ***$p < 0.001$. **E** Length of cytoophidia in ovary nurse cell. We analyzed 94 filaments in control group and 94 filaments in myosin inhibited. Data are represented as mean ± SEM, **$p < 0.01$. **F** Relative mRNA levels of control and myosin inhibitor-treated are measured by quantitative RT-PCR (6 ovaries/group, 3 biological replicates). Data are represented as mean ± SEM. ns, no significance. **G** Intensity of CTPS-mCherry signal in cytoophidia (ns, no significance in difference). 3 ovaries in control group and 3 ovaries in myosin inhibited group are analyzed. Data are represented as mean ± SEM.

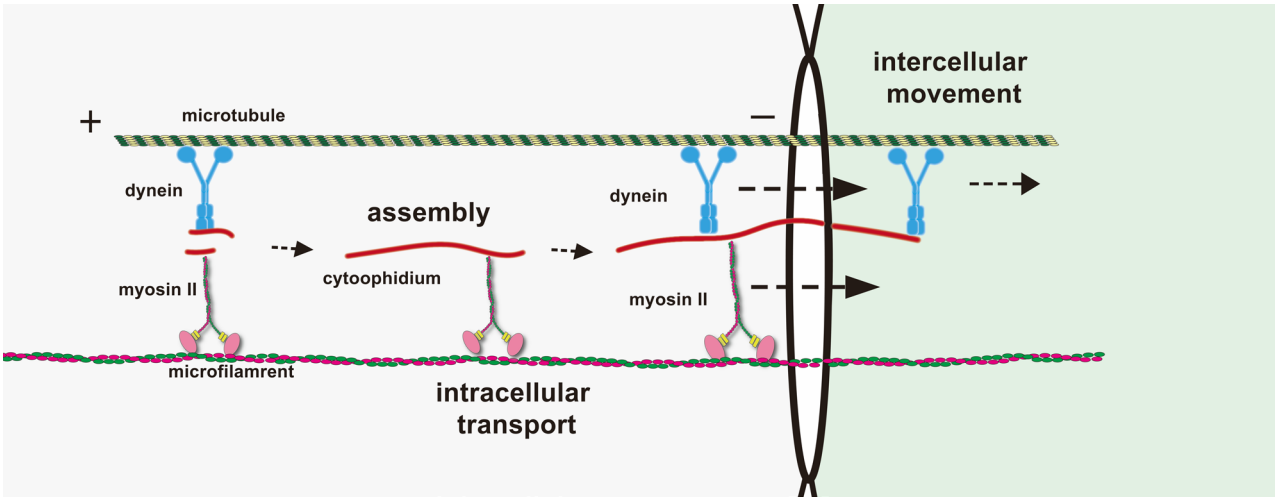

Fig. 8 Dynamic Regulation Model of Cytoophidia Dynamics. The diagram of a working model for cytoophidia dynamics. Under physiological conditions, the morphology of cytoophidia is variable. In addition, cytoophidia exhibit two distinct modes of transport: intracellular movement and intercellular movement. Microfilament and microtubules mediate the active transport of cytoophidia. Dynein and myosin are responsible for intercellular transport of cytoophidia from the nurse cells to the oocyte.

Supplementary Information

The online version contains supplementary material available at https://doi.org/10.1186/s13578-026-01530-1.

Supplementary Material 1

Supplementary Material 2

Supplementary Material 3

Supplementary Material 4

Supplementary Material 5

Supplementary Material 6

Supplementary Material 7

Supplementary Material 8

Acknowledgements

We thank the Molecular Imaging Core Facility (MICF) and Molecular Cell Core Facility (MCCF) at the School of Life Science and Technology, ShanghaiTech University for providing technical support. We thank the Core Facility of *Drosophila* Resource and Technology, Center for Excellence in Molecular Cell Science, Chinese Academy of Sciences.

Authors' contributions

X.-J. Liu: Conceptualization, Methodology, Investigation, Formal Analysis, Writing—Original Draft, and Visualization. Y.-L. Li: Conceptualization, Advising, Writing—Review and Editing. S.-Y. Pang: Investigation. K. Dou.: Resources, Writing—Review, Advising. J.-L. Liu: Conceptualization, Resources, Writing—Review and Editing, Supervision, and Project Administration. All authors have read and agreed to the published version of the manuscript.

Funding

This work was supported by the grants from the Ministry of Science and Technology of China (No. 2021YFA0804700), National Natural Science Foundation of China (Grant Nos. 32370744 and 32350710195), and UK Medical Research Council (Grant Nos. MC_UU_12021/3 and MC_U137788471) for grants to J. L. L. and National Natural Science Foundation of China (Grant No. 32370604) to K.D.

Data availability

All data are available in the text and supplementary information. Original data are available upon request.

Declarations

Competing interests

The authors declare no conflicts of interest.

Received: 27 September 2025 / Accepted: 30 December 2025
Published online: 13 February 2026

References

1. Lieberman I. Enzymatic amination of uridine triphosphate to cytidine triphosphate. J Biol Chem. 1956;222(2):765–75.
2. Liu J-L. Intracellular compartmentation of CTP synthase in *Drosophila*. J Genet Genomics. 2010;37(5):281–96.
3. Ingerson-Mahar M, Briegel A, Werner JN, Jensen GJ, Gitai Z. The metabolic enzyme CTP synthase forms cytoskeletal filaments. Nat Cell Biol. 2010;12(8):739–46.
4. Noree C, Sato BK, Broyer RM, Wilhelm JE. Identification of novel filament-forming proteins in *Saccharomyces cerevisiae* and *Drosophila melanogaster*. J Cell Biol. 2010;190(4):541–51.
5. Chen K, Zhang J, Tastan ÖY, Deussen ZA, Siswick MY, Liu JL.Glutamine analogs promote Cytoophidium assembly in human and *Drosophila* cells. J Genet Genomics. 2011;38(9):391–402.
6. Carcamo WC, Satoh M, Kasahara H, Terada N, Hamazaki T, Chan JY, Yao B, Tamayo S, Covini G, von Mühlen CA, Chan EK.Induction of cytoplasmic rods and rings structures by Inhibition of the CTP and GTP synthetic pathway in mammalian cells. PLoS ONE. 2011;6(12):e29690.
7. Zhang J, Hulme L, Liu JL. Asymmetric inheritance of cytoophidia in *Schizosaccharomyces Pombe*. Biol Open. 2014;3(11):1092–7.
8. Daumann M, Hickl D, Zimmer D, DeTar RA, Kunz HH, Möhlmann T. Characterization of filament-forming CTP synthases from *Arabidopsis Thaliana*. Plant J. 2018;96(2):316–28.
9. Zhou S, Xiang H, Liu JL. CTP synthase forms cytoophidia in archaea. J Genet Genomics. 2020;47(4):213–23.
10. Liu JL. The enigmatic cytoophidium: compartmentation of CTP synthase via filament formation. BioEssays. 2011;33(3):159–64.
11. Aughey GN, Liu JL. Metabolic regulation via enzyme filamentation. Crit Rev Biochem Mol Biol. 2015;51(4):282–93.

12. Liu JL. The Cytoophidium and its kind: filamentation and compartmentation of metabolic enzymes. Annu Rev Cell Dev Biol. 2016;32:349–72.
13. Sun Z, Liu J-L. Forming cytoophidia prolongs the half-life of CTP synthase. Cell Discovery. 2019;5(1):32.
14. Zhang, Y.; Liu, J.-L. The Impact of Developmental and Metabolic Cues on Cytoophidium Formation. Int. J. Mol. Sci. 2024, 25, 10058
15. Zhang Y, Liu J, Liu J-L. The atlas of cytoophidia in *Drosophila* larvae. J Genet Genomics. 2020;47(6):321–31.
16. Li Y-L, Liu J-L. Cytoophidium complexes resonate with cell fates. Cell Mol Life Sci. 2025;82(1):54.
17. Liu J, Zhang Y, Zhou Y, Wang QQ, Ding K, Zhao S, Lu P, Liu JL. Cytoophidia coupling adipose architecture and metabolism. Cell Mol Life Sci. 2022;79(10):534.
18. Wang Q-Q, You D-D, Liu J-L. Cytoophidia maintain the integrity of *Drosophila* follicle epithelium. Int J Mol Sci. 2022;23(23):15282.
19. Li H, Ye F, Ren JY, Wang PY, Du LL, Liu JL. Active transport of cytoophidia in *Schizosaccharomyces pombe*. FASEB J. 2018;32(11):5891–8.
20. Peng M, Chang CC, Liu JL, Sung LY. CTPS and IMPDH form cytoophidia in developmental thymocytes. Exp Cell Res. 2021;405(1):112662.
21. Chang CC, Jeng YM, Peng M, Keppeke GD, Sung LY, Liu JL. CTP synthase forms the Cytoophidium in human hepatocellular carcinoma. Exp Cell Res. 2017;361(2):292–9.
22. Zhou X, Guo CJ, Chang CC, Zhong J, Hu HH, Lu GM, Liu JL. Structural basis for ligand binding modes of CTP synthase. Proc Natl Acad Sci. 2021;118(30):e2026621118.
23. Guo CJ, Liu JL. Cytoophidia and filaments: you must unlearn what you have learned. Biochem Soc Trans. 2023;51(3):1245–56.
24. Liu JL. Primary partitioning principles of the cell: Cytoophidium assembly, phase separation and membrane enclosure. Exp Cell Res. 2025;452(2):114766.
25. Wang Q, Liu J-L, Liu J. CTPS cytoophidia in *Drosophila*: distribution, regulation, and physiological roles. Exp Cell Res. 2025;447(2):114536.
26. Simonet JC, Foster MJ, Lynch EM, Kollman JM, Nicholas E, O'Reilly AM, Peterson JR . CTP synthase polymerization in germline cells of the developing *Drosophila* egg supports egg production. Biology Open, 2020: p. bio.050328.
27. Wu Z, Liu J-L. Cytoophidia respond to nutrient stress in *Drosophila*. Exp Cell Res. 2019;376(2):159–67.
28. Bandyadka S, Lebo DPV, Mondragon AA, Serizier SB, Kwan J, Peterson JS, Chasse AY, Jenkins VK, Calikyan A, Ortega AJ, Campbell JD, Emili A, McCall K. Multi-modal comparison of molecular programs driving nurse cell death and clearance in *Drosophila melanogaster* oogenesis. PLoS Genet. 2025 Jan 3;21(1):e1011220.
29. Welte MA, Gross SP, Postner M, Block SM, Wieschaus EF.Developmental regulation of vesicle transport in *Drosophila* embryos: forces and kinetics. Cell. 1998;92(4):547–57.
30. Deng W, Lin H. Spectrosomes and fusomes anchor mitotic spindles during asymmetric germ cell divisions and facilitate the formation of a polarized microtubule array for oocyte specification In*Drosophila*. Dev Biol. 1997;189(1):79–94.
31. Bastock R, St Johnston D. *Drosophila* Oogenesis Curr Biology. 2008;18(23):R1082–7.
32. Navarro-Costa P, McCarthy A, Prudêncio P, Greer C, Guilgur LG, Becker JD, Secombe J, Rangan P, Martinho RG. Early programming of the oocyte epigenome temporally controls late prophase I transcription and chromatin remodelling. Nat Commun. 2016;7(1):12331.
33. Giedt MS, Tootle TL. The vast utility of *Drosophila* oogenesis. Methods Mol Biol. 2023;2626:1–36.
34. McLaughlin JM, Bratu DP. *Drosophila melanogaster* Oogenesis: An Overview, in *Drosophila* Oogenesis, D.P. Bratu and G.P. McNeil, Editors. 2015, Springer New York: New York, NY. pp. 1–20.
35. Fletcher DA, Mullins RD. Cell mechanics and the cytoskeleton. Nature. 2010;463(7280):485–92.
36. Januschke J, Gervais L, Dass S, Kaltschmidt JA, Lopez-Schier H, St Johnston D, Brand AH, Roth S, Guichet A. Polar transport in the *Drosophila* Oocyte requires dynein and Kinesin I Cooperation. Curr Biol. 2002;12(23):1971–81.
37. Carlton JG, Jones H, Eggert US. Membrane and organelle dynamics during cell division. Nat Rev Mol Cell Biol. 2020;21(3):151–66.
38. Adaptive microtubule reinforcement enables cell migration through 3D environments. Nat Cell Biol, 2024. 26(9): pp. 1382–3.
39. Yildiz A. Sorting out microtubule-based transport. Nat Rev Mol Cell Biol. 2021;22(2):73–73.
40. Markus SM. Microtubule motors of opposite Polarity cooperate rather than compete in cargo transport. Nat Struct Mol Biol. 2025;32(4):595–7.
41. Karki S, Holzbaur ELF. Cytoplasmic dynein and dynactin in cell division and intracellular transport. Curr Opin Cell Biol. 1999;11(1):45–53.
42. Hirokawa N, Noda Y, Tanaka Y, Niwa S. Kinesin superfamily motor proteins and intracellular transport. Nat Rev Mol Cell Biol. 2009;10(10):682–96.
43. Qu J, Li J, Wang H, Lan J, Huo Z, Li X . Decoding the role of microtubules: a trafficking road for vesicle. Theranostics. 2025;15(11):5138–5
44. Yildiz A. Mechanism and regulation of Kinesin motors. Nat Rev Mol Cell Biol. 2025;26(2):86–103.
45. Liu B, Liu C, Li Z, Liu W, Cui H, Yuan J. A subpellicular microtubule dynein transport machinery regulates Ookinete morphogenesis for mosquito transmission of *Plasmodium yoelii*. Nat Commun. 2024;15(1):8590.
46. Kneussel M, Wagner W. Myosin motors at neuronal synapses: drivers of membrane transport and actin dynamics. Nat Rev Neurosci. 2013;14(4):233–47.
47. Zhang B, Zhang Y, Liu J-L. Highly effective proximate labeling in *Drosophila*. G3 Genes|Genomes|Genetics, 2021. 11(5).
48. Brand AH, Perrimon N. Targeted gene expression as a means of altering cell fates and generating dominant phenotypes. Development. 1993;118(2):401–15.
49. Drechsler M, Giavazzi F, Cerbino R, Palacios IM . Active diffusion and advection in *Drosophila* oocytes result from the interplay of actin and microtubules. Nat Commun. 2017;8(1):1520.
50. ang HJ, Kim YY, Lee KM, Shin JE, Yun J . The PINK1 activator niclosamide mitigates mitochondrial dysfunction and thermal hypersensitivity in a Paclitaxel-Induced *Drosophila* model of peripheral neuropathy. Biomedicines, 2022. 10(4).
51. Townsley FM, Bienz M. Actin-dependent membrane association of a *Drosophila* epithelial APC protein and its effect on junctional armadillo. Curr Biol. 2000;10(21):1339–48.
52. Gollapudi SK, Ma W, Chakravarthy S, Combs AC, Sa N, Langer S, Irving TC, Nag S. Two classes of myosin Inhibitors, Para-nitroblebbistatin and Mavacamten, stabilize β-Cardiac myosin in different structural and functional States. J Mol Biol. 2021;433(23):167295.
53. Firestone AJ, Weinger JS, Maldonado M, Barlan K, Langston LD, O'Donnell M, Gelfand VI, Kapoor TM, Chen JK. Small-molecule inhibitors of the AAA + ATPase motor cytoplasmic dynein. Nature. 2012;484(7392):125–9.
54. Rothman JE. Mechanisms of intracellular protein transport. Nature. 1994;372(6501):55–63.
55. Januschke J, Gervais L, Dass S, Kaltschmidt JA, Lopez-Schier H, St Johnston D, Brand AH, Roth S, Guichet A. Polar transport in the *Drosophila* oocyte requires dynein and Kinesin I Cooperation. Curr Biol. 2002;12(23):1971–81.
56. Duncan JE, Warrior R. The cytoplasmic dynein and Kinesin motors have interdependent roles in patterning the *Drosophila* oocyte. Curr Biol. 2002;12(23):1982–91.
57. Cohen RS. Oocyte patterning: dynein and Kinesin, inc. Curr Biol. 2002;12(23):R797–9.
58. Wollscheid H-P, Ulrich HD. Chromatin Meets the cytoskeleton: the importance of nuclear actin dynamics and associated motors for genome stability. DNA Repair. 2023;131:103571.
59. Vasquez CG, Heissler SM, Billington N, Sellers JR, Martin AC . *Drosophila* non-muscle myosin II motor activity determines the rate of tissue folding. Elife, 2016. 5.
60. Aldaz S, Escudero LM, Freeman M. Dual role of myosin II during *Drosophila* imaginal disc metamorphosis. Nat Commun. 2013;4(1):1761.
61. Bearne SL, Guo C-J, Liu J-L. GTP-Dependent regulation of CTP synthase: evolving insights into allosteric activation and NH3 translocation. Biomolecules. 2022;12(5):647.
62. Lynch EM, Hicks DR, Shepherd M, Endrizzi JA, Maker A, Hansen JM, Barry RM, Gitai Z, Baldwin EP, Kollman JM. Human CTP synthase filament structure reveals the active enzyme conformation. Nat Struct Mol Biol. 2017;24(6):507–14.
63. Zhou X, Guo CJ, Hu HH, Zhong J, Sun Q, Liu D, Zhou S, Chang CC, Liu JL. *Drosophila* CTP synthase can form distinct substrate- and product-bound filaments. J Genet Genomics. 2019;46(11):537–45.
64. Zhou X, Guo CJ, Chang CC, Zhong J, Hu HH, Lu GM, Liu JL . Structural basis for ligand binding modes of CTP synthase. Proc Natl Acad Sci U S A, 2021. 118(30).
65. McIntosh BB, Pyrpassopoulos S, Holzbaur ELF, Ostap EM . Opposing Kinesin and Myosin-I motors drive membrane deformation and tubulation along engineered cytoskeletal networks. Curr Biol. 2018;28(2):236–e2485.
66. Nicolas E, Chenouard N, Olivo-Marin JC, Guichet A . A dual role for actin and microtubule cytoskeleton in the transport of golgi units from the nurse cells to the oocyte across ring canals. Mol Biol Cell. 2009;20(1):556–68.

67. Schroer TA, Sheetz MP. Two activators of microtubule-based vesicle transport. J Cell Biol. 1991;115(5):1309–18.
68. Reck-Peterson SL, Redwine WB, Vale RD, Carter AP. The cytoplasmic dynein transport machinery and its many cargoes. Nat Rev Mol Cell Biol. 2018;19(6):382–98.
69. Carter AP, Diamant AG, Urnavicius L. How dynein and dynactin transport cargos: a structural perspective. Curr Opin Struct Biol. 2016;37:62–70.
70. Bullock SL, Ish-Horowicz D. Conserved signals and machinery for RNA transport in *Drosophila* oogenesis and embryogenesis. Nature. 2001;414(6864):611–6.
71. Weil TT. mRNA localization in the *Drosophila* germline. RNA Biol. 2014;11(8):1010–8.
72. Dienstbier M, Boehl F, Li X, Bullock SL. Egalitarian is a selective RNA-binding protein linking mRNA localization signals to the dynein motor. Genes Dev. 2009;23(13):1546–58.
73. Clark A, Meignin C, Davis I. A Dynein-dependent shortcut rapidly delivers axis determination transcripts into the *Drosophila* oocyte. Development. 2007;134(10):1955–65.
74. Lu W, Lakonishok M, Gelfand VI. Gatekeeper function for short stop at the ring canals of the *Drosophila* ovary. Curr Biol. 2021;31(15):3207–e32204.

Publisher's note